Journal of Visualization, Vol. 3, No. 3 (2000) 287-294

Numerical Simulation of Wave Effects around Compound Coastal Structures

Chen, H. C.*1 and Lin, W. M.*2

*1 Ocean Engineering Program, Department of Civil Engineering, Texas A&M University, College Station, TX 77843-3136, USA.
*2 Ship Technology Division, Science Applications International Corporation, Annapolis, MD 21401, USA.

Received 28 January 2000.
Revised 21 February 2000.

***Abstract*:** A new three-dimensional potential flow numerical method has been developed to study wave diffraction around compound coastal structures. This new method is based on a multi-block finite-analytic scheme. A chimera domain decomposition technique is used to model complex geometry and to connect overlapped grids by interpolating information across block boundaries. Calculations were performed for three examples, including a harbor entrance, a single breakwater, and a combined breakwater and large floating platform, to illustrate the flexibility and effectiveness of the present method.

***Keywords*:** Laplace equation, unsteady flow, time-domain simulation, multi-block method, chimera domain decomposition, breakwater, floating platform, harbor.

1. Introduction

Very large floating structures in the coastal area have recently been considered for use as an airport. The platform can be on the order of several thousand meters long. This type of platform typically requires the protection of a breakwater from severe weather conditions. For the design of a large platform, the wave field behind the breakwater is one of the most important design considerations. The breakwater must be designed to achieve the specified design waves for the platform. Therefore, the breakwater efficiency has to be established carefully.

Computational methods are available for computing the propagation of a typhoon wind/wave from the open ocean to the shore and to compute the relationship between the wave field outside and inside the breakwater. However, these methods typically ignore the interaction between the breakwater and the platform. Furthermore, large-domain computations for this type of platform are still not practical in actual designs due to geometry complexity and prohibitively high computation cost.

In this study, an efficient three-dimensional unsteady numerical method, CHAMPS (CHimera finite Analytic Method Potential-flow Solver), was developed to compute the wave mitigation behind a breakwater and the wave field around a combined breakwater and platform configuration. This new method solves the Laplace equation on structured multi-block grids using the finite-analytic method of Chen, Patel, and Ju (1990). Within each computational block, velocity potential was solved on a general curvilinear, body-fitted coordinate system. This method is an extension of Chen and Lee (1996, 1999) for calculations of fully nonlinear free surface flows generated by bodies moving in calm water.

For body-wave interaction problems, the incident ambient wave field is generated by a numerical wavemaker. For fully nonlinear wave cases, the nonlinear free surface boundary conditions can be enforced on the exact free surface for accurate resolution. For weakly nonlinear wave cases, the nonlinear free surface boundary

conditions may be specified on the mean free surface to reduce the simulation time. Wave effects on the structure can be calculated by the unsteady pressure field. This information can be used for further structural analysis.

For modeling complex geometries, a chimera domain decomposition technique has been incorporated to connect embedded, patched, or overlapped grids by interpolating information across block boundaries. The chimera scheme provides a very effective and flexible treatment of complex geometries and flow conditions in multiply-connected flow domains, since each component grid can be generated separately and linked in arbitrary combinations. Moreover, selective grid refinements can be efficiently performed in areas of high gradients without a significant increase in total CPU time. The method is very general and can model both the bottom topography and shorelines in addition to the physical structures. A more detailed description of the chimera domain decomposition approach is given in Chen and Chen (1998) and Chen and Liu (1999).

Three examples are given in this paper to demonstrate the effectiveness of this new method. The first example is a classical diffraction problem of waves through a single gap in a breakwater. The second example is the wave diffraction behind a finite width breakwater. The third example is a combined breakwater and floating platform configuration. The third example clearly illustrates the necessity of using a chimera scheme for design assessment of different breakwater and platform arrangements.

2. Theoretical Formulation

For the simple breakwaters and combined breakwater and platform configurations considered here, the associated boundary value problem can be constructed using a Cartesian coordinate system $x^i = (x, y, z)$. The regular waves generated by the wavemaker are traveling in the x direction, and the z-axis is pointing upward with $z = 0$ representing the mean water surface. It is assumed that the fluid is incompressible and inviscid and that the flow is irrotational. This implies the existence of a velocity potential function $\phi(x, y, z, t)$ such that the velocity can be described by $V=\nabla\phi$. Due to the conservation of fluid mass, the velocity potential ϕ satisfies the Laplace equation:

$$\nabla^2\phi = 0 \tag{1}$$

Also, the momentum equations reduce to the Bernoulli's equation

$$p + \phi_t + \frac{1}{2}\nabla\phi \bullet \nabla\phi = 0 \tag{2}$$

where p is the dynamic pressure.

On the free surface, the normal velocity of a point on the wave surface should be equal to the normal velocity of a fluid particle at that point. This kinematic free surface boundary condition can be expressed as

$$\eta_t + \phi_x\eta_x + \phi_y\eta_y - \phi_z = 0 \quad \text{on} \quad z = \eta \tag{3}$$

where η is the wave elevation. For the inviscid fluid, the dynamic free surface condition requires that the normal pressure on the free surface be equal to the atmospheric pressure. When both the viscosity and surface tension are neglected, the dynamic condition on the exact free surface can be written as

$$\phi_t + \frac{1}{2}\nabla\phi \bullet \nabla\phi + \frac{\eta}{Fr^2} = 0 \quad \text{on} \quad z = \eta \tag{4}$$

where Fr is the Froude number $U_o/\sqrt{gL}$ based on a reference velocity U_o, a reference length L, and the gravitational acceleration g.

On the wetted body surface, the normal velocity of a point on the body must be equal to the normal velocity of the adjacent fluid, $V \quad n = V_s \quad n$, where V and V_s are the fluid and body velocities, respectively, and n is the unit normal of the body surface. The same Neumann boundary conditions has also been used for the bottom and side wall boundaries. On the upstream boundary, the velocity potential for the incident wave is specified:

$$\phi = \sum_{n=1}^{\infty} \frac{A_n}{\omega_n} \frac{\cosh k_n(h+z)}{\cosh k_n h} \sin\left[k_n(x\cos\theta_n + y\sin\theta_n) - \omega_n t + \varepsilon_n\right] \tag{5}$$

where A_n is the wave amplitude, h is the water depth, k_n is the wave number, ω_n is the wave frequency, θ_n is the wave heading, and ε_n is the phase shift.

In the far field, a radiation condition or absorbing beach must be employed to avoid wave reflections from the downstream boundary. Open boundaries enclosing the fluid domain are artificial and essentially arbitrary. The

fluid domain is truncated at some distance from the fluid region of interest. Physically, the aim of the radiation boundary condition is to eliminate unphysical wave reflections from the open boundaries; otherwise, those reflected waves would interact with the waves inside the solution domain and contaminate the solution. Several methods, such as the Rayleigh viscosity method, the sponge layer method (Chan, 1977), and Sommerfeld's radiation condition (Orlanski, 1976; Chan, 1977), have been considered for the handling of radiation conditions on open boundaries. In this study, Sommerfeld's radiation condition has been used to eliminate wave reflection from the downstream boundary.

To formulate Sommerfeld's condition in unsteady flow, it is assumed that the wave profile is of the form of $Q(k_x x + k_y y - \omega t)$, with Q representing ϕ or η. Here, k_x and k_y denote wave numbers in x and y directions, respectively. ω is the wave frequency. In the present study, the upwind-centered finite-difference scheme of Chan (1977) was employed for discretization of the radiation conditions. A detailed description on the numerical implementation of the radiation condition is given in Chen and Lee (1996, 1999).

3. Chimera Laplace Solver

In the present chimera Laplace method, the solution domain is first decomposed into a number of computational blocks. The body-fitted numerical grids for different part of the geometry are generated separately. The PEGSUS program of Suhs and Tramel (1991) was employed to determine the interpolation information for linking grids. It outputs a complete set of information corresponding to the interpolation performed. The most important information is included in a "blanking" array, the interpolation and boundary lists, the interpolation stencils, and the maps showing boundary and interpolation node locations. The "blanking" array and interpolation stencils are incorporated into the present flow solver to remove hole points and update boundary conditions from the linking grids.

Within each computational block, the finite-analytic method of Chen, Patel, and Ju (1990) was employed to solve the Laplace equation for velocity potential on a general curvilinear, body-fitted coordinates system. For fully nonlinear free surface flows, the wave elevation was updated for each time step using the kinematic free surface boundary condition (3) while the dynamic free surface boundary condition (4) had been enforced on the exact free surface. In the present study, however, we shall simplify the solution procedure by applying the nonlinear free surface boundary conditions (3) and (4) on the mean free surface. Since the computational domain and numerical grids remain fixed under this approximation, it enables us to use the same geometric coefficients and PEGSUS interpolation stencils throughout the entire simulation.

In addition to the first-order Euler implicit method used in Chen and Lee (1996, 1999) for steady-state wave calculations, the CHAMPS code also incorporated several higher-order integration schemes that are more appropriate for time-domain wave simulations. In particular, we have performed extensive calculations using the fourth-order Adams-Bashforth-Moulton predictor-corrector method, the classical fourth-order Runge-Kutta method, and the fifth-order Runge-Kutta-Fehlberg method to evaluate the general performance of these higher-order methods. The results indicated that the Runge-Kutta-Fehlberg method is the most stable and accurate time-integration scheme for wave-body interaction problems considered here. Therefore, we shall present only the results obtained from the Runge-Kutta-Fehlberg method in the next section.

4. Results and Discussions

Three numerical simulation results are given in this section to demonstrate the effectiveness of the present method. The first example is a classical diffraction problem of waves through a single gap in a breakwater. This case is similar to wave entrance into a harbor. In this computation, the water depth is set to be constant at 25 meters. The length of the breakwater is 500 meters each side and the harbor opening is 250 meters. The total computation domain is 1,250 meters in length and 1,250 meters in width.

Figure 1(a) shows the computational grid on the free surface. For each one of the breakwater, there are 30,000 numerical elements (100 30 10). The entire background computation domain has 144,000 elements (240 60 10). The advantage of the multi-block chimera scheme is quite obvious here. The background grid and the two breakwater grids intersect each other, and the chimera scheme can automatically blank out the unnecessary grids and perform solution interpolation across the block boundaries.

For actual simulation, a shallow water plane progressive wave is sent in from the left-hand-side of the fluid domain. The wave length in this case is 125 meters (half of the harbor opening) and the wave amplitude is 0.5

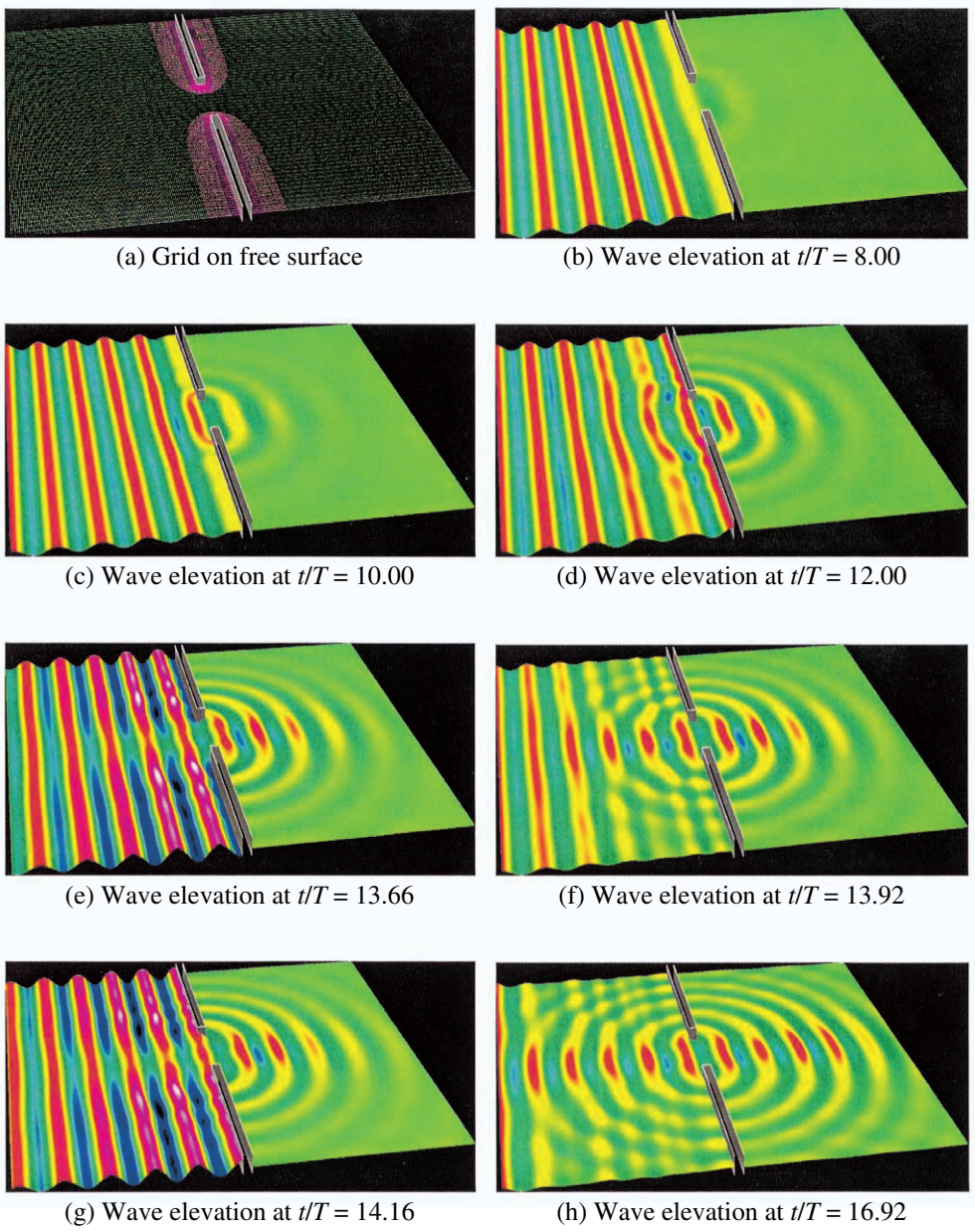

(a) Grid on free surface

(b) Wave elevation at $t/T = 8.00$

(c) Wave elevation at $t/T = 10.00$

(d) Wave elevation at $t/T = 12.00$

(e) Wave elevation at $t/T = 13.66$

(f) Wave elevation at $t/T = 13.92$

(g) Wave elevation at $t/T = 14.16$

(h) Wave elevation at $t/T = 16.92$

Fig. 1. CHAMPS simulation of wave diffraction through a single gap in a breakwater.

meter. Calculations were performed for 900 time steps using a constant time increment of $0.02T$, where T is the period of the incident wave. A movie which contains the entire time series of free surface water elevations was made to facilitate a detailed visualization of the diffraction wave patterns. For the sake of brevity, we shall present the wave patterns at seven different time instances of the simulation as shown in Fig. 1. The interaction between the diffracted and reflected waves with the incident wave produced rather complex wave patterns in front of the breakwaters. Figures 1(e) to 1(g) are plotted with an interval of quarter wave period ($T/4$). The existence of standing waves in front of the breakwater can be seen clearly by the interesting wave superposition and cancellation phenomena of the reflection and incident waves. At $t/T = 13.92$ and 16.92, the reflected wave and the incident wave cancelled each other almost completely. Consequently, a nearly symmetric diffraction wave pattern was observed ahead and behind the breakwater. The computed free surface wave patterns are quite similar to the classical wave diffraction results of Penny and Price (1952).

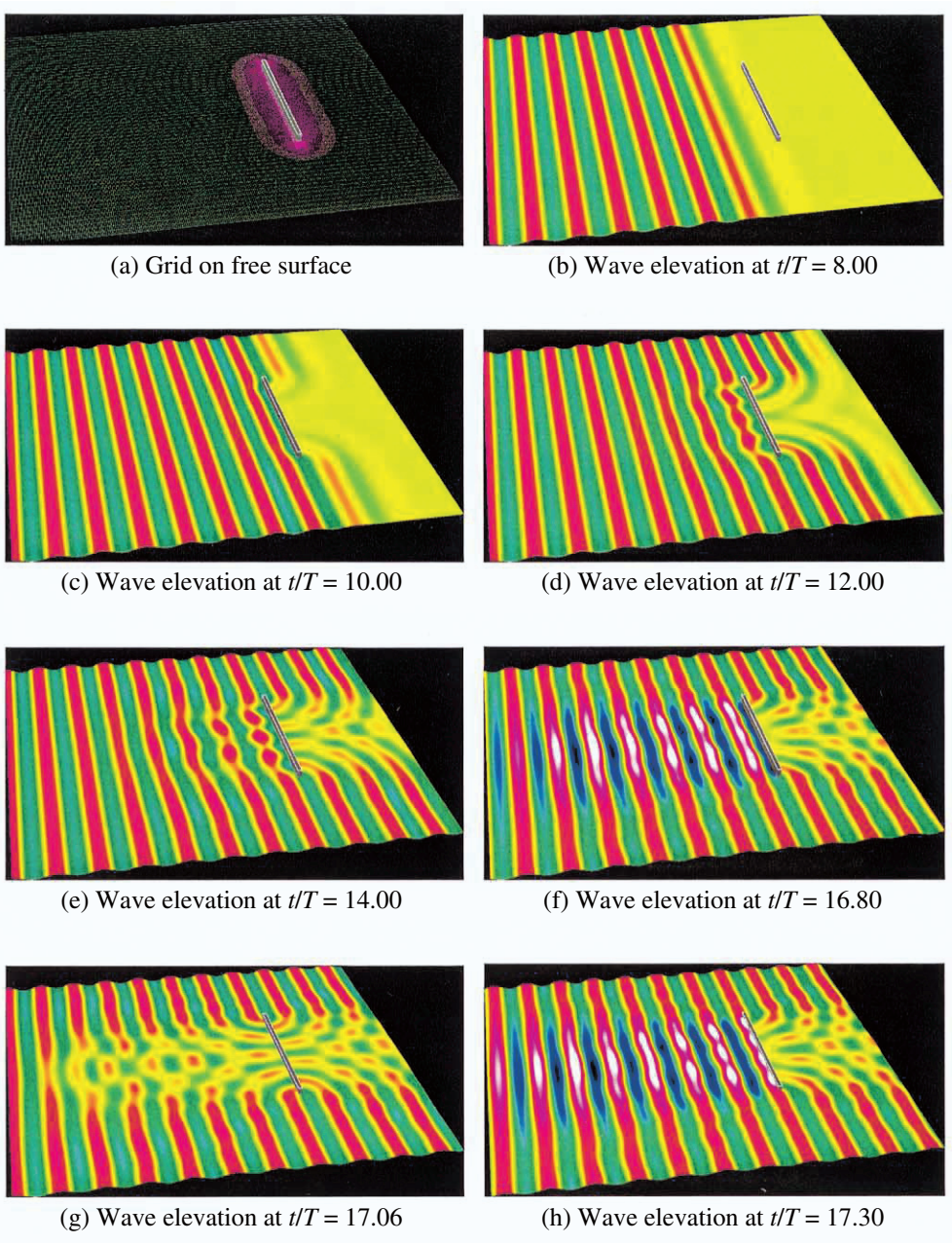

(a) Grid on free surface

(b) Wave elevation at $t/T = 8.00$

(c) Wave elevation at $t/T = 10.00$

(d) Wave elevation at $t/T = 12.00$

(e) Wave elevation at $t/T = 14.00$

(f) Wave elevation at $t/T = 16.80$

(g) Wave elevation at $t/T = 17.06$

(h) Wave elevation at $t/T = 17.30$

Fig. 2. CHAMPS simulation of wave diffraction behind a finite width breakwater.

The second example is a simple breakwater of rectangular cross-section resting on a bottom of constant water depth at 25 meters. This example is used to demonstrate the efficiency of a finite width breakwater. The breakwater is 25 meters wide and 1,000 meters long in this computation. The computation domain is 2,500 meters 2,500 meters as shown in Fig. 2(a). Again, the chimera scheme is used with 60,000 elements (200 30 10) around the breakwater and 144,000 elements (240 60 10) on the background computation domain.

As shown in Fig. 2, a regular plane progressive wave (wave length of 250 meters) is coming from the left (a direction normal to the breakwater). Time-domain simulations were performed for 20 wave periods (1,000 time steps) using a constant time increment of $0.02T$. An animation movie was again made to provide a thorough understanding of the complex interaction between the diffraction, reflection, and the incident wave system. Figures 2(f) to 2(h) are plotted at an interval of quarter wave period ($T/4$). At $t/T = 16.80$ and 17.30, large amplitude standing waves were observed in front of the breakwater as a result of the superposition of the incident and reflected waves. The cancellation between the incident and the reflection waves can also be clearly seen at $t/T = 17.06$. In addition, ring waves are formed in front of and behind the breakwater. These ring waves are caused by

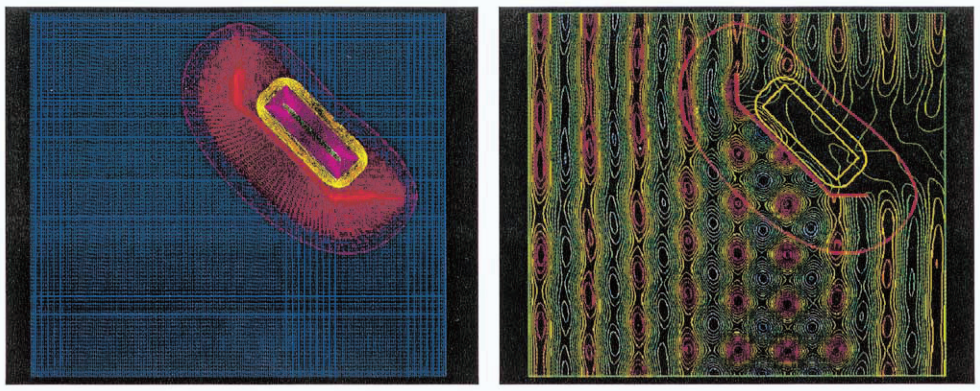

(a) Grid on combined configuration

(b) Velocity potential at $t/T = 12.00$

(c) Wave elevation at $t/T = 6.00$

(d) Wave elevation at $t/T = 8.00$

(e) Wave elevation at $t/T = 10.00$

(f) Wave elevation at $t/T = 12.00$

Fig. 3. CHAMPS simulation of wave field for a combined breakwater and platform configuration.

the interference of the diffracted waves traveling across the center plane of symmetry to the opposite side of the breakwater. It is further noted that the amplitude of the diffracted waves behind the breakwater is significantly lower than the incident wave amplitude for the entire animation sequence. This clearly illustrated the efficiency of the breakwater in reducing the amplitude and energy of the incident waves.

The third example is a combined platform and breakwater configuration. As shown in Fig. 3(a), the geometry for this combined model is a breakwater in three sections and a large floating platform behind it. The total length of the breakwater is 3,125 meters and the floating platform is 1,500 meters 450 meters 5 meters. The water depth is constant at 25 meters in this computation. In a typical near-shore airfield configuration, there is shoreline behind the platform, although a shoreline is not modeled in this computation.

The complete computation domain is 6,000 meters 5,250 meters. Only the grids near the breakwater and the floating platform are shown in Fig. 3(a). Five overlapped blocks were used for this complex configuration. The background grid block covering the entire computation domain has 200 100 10 numerical elements; the second grid block is around the breakwater and has 194 34 10 elements; the third grid block is around the platform and has 122 14 10 elements; the fourth grid block is below the platform and has 122 16 8

elements; and the fifth grid block is a branch cut of the grid block below the platform and has 60 3 9 numerical elements. These five grids intersect each other and the chimera scheme was used in the CHAMPS method to automatically blank out the intersecting grid points in the calculation.

Figure 3 presents the result of a wave diffraction computation with a plane progressive wave of 750 meters (wave length) 5 meters (wave height) sent in from one side of the breakwater. Time-domain calculations were performed for 12 wave periods with a constant time increment of $0.02T$. Several animation movies were made to examine both the wave patterns and velocity potential contours in different regions of the combined breakwater and platform configuration. Figure 3(b) shows the contours of the velocity potential at $t/T = 12.0$ to illustrate the general wave pattern. In addition, an animation sequence was shown in Figs. 3(c) - 3(f) for wave diffraction in front and behind the breakwater as well as the interaction between the breakwater and the large platform. The result gives a clear picture of the wave propagation along the breakwater and the formation of the ring waves due to the interaction of the incident and reflection waves. The most severe wave effect on the platform is on the upper left-hand corner of the platform. The wave height there is about 1/3 of the incident wave height.

A particularly interesting result is observed in Fig. 3(b), where the velocity potential in the flow domain at $t/T = 12.0$ is given. This top view clearly shows that the "ring" waves are actually very close to square in shape. This is the result of interaction between the incident waves and reflection waves by the 45-degree breakwater (the longest piece of breakwater). The thick lines around the floating platform and around the combined configuration are the boundaries of the embedded grid blocks. The continuity of the solution across the block boundaries is clearly evident. With the flexibility and effectiveness of the chimera domain decomposition approach, the CHAMPS method can be readily generalized for time-domain simulation of other coastal or offshore structures.

5. Conclusion

A three-dimensional potential flow numerical method is presented for studying nonlinear wave diffraction around complex geometries. With the chimera domain decomposition technique, the modeling of complex geometries in advanced numerical simulations is now becoming practical. The examples presented in this study demonstrate the effectiveness of this new numerical method. Some interesting wave interactions are observed, including superposition and cancellation of incident and reflection waves, and the formation of square-shaped ring waves. For design assessment of the large floating platform, this method provides complete flow field information, including the interaction between the breakwater and the floating platform. Wave loads on the platform can be computed from the pressure field and hydro-elastic effects of the platform can be examined.

Acknowledgments

The research is partially funded by an IR&D project of Science Applications International Corporation. All computations were performed on the CRAY C-90 of Cray Research Inc. at Eagen, Minnesota, under the sponsorship of Frank Kampe.

References

Chan, R. K. C., Finite-Difference Simulation of the Planar Motion of a Ship, Proceedings of the 2nd International Conference on Numerical Ship Hydrodynamics (University of California, Berkeley), (1977), 39-52.

Chen, H. C. and Chen, M., Chimera RANS Simulation of a Berthing DDG-51 Ship in Translational and Rotational Motions, International Journal of Offshore and Polar Engineering, 8-3 (1998), 182-191.

Chen, H. C., and Lee, S. K., Interactive RANS/LAPLACE Method for Nonlinear Free Surface Flows, Journal of Engineering Mechanics, 122-2 (1996), 153-162.

Chen, H. C. and Lee, S. K., RANS/LAPLACE Simulations of Nonlinear Waves Induced by Surface-Piercing Bodies, Journal of Engineering Mechanics, 125-11 (1999), 1231-1242.

Chen, H. C. and Liu, T., Turbulent Flow Induced by a Full-Scale Ship in Harbor, Journal of Engineering Mechanics, 125-7 (1999), 827-835.

Chen, H. C., Patel, V. C. and Ju, S., Solutions of Reynolds-Averaged Navier-Stokes Equations for Three-Dimensional Incompressible Flows, Journal of Computational Physics, 88-2 (1990), 305-336.

Orlanski, I., A Simple Boundary Condition for Unbounded Hyperbolic Flows, Journal of Computational Physics, 21 (1976), 251-269.

Penney, W. G. and Price, A. T., The Diffraction Theory of Sea Waves and the Shelter Afforded by Breakwater, Philos, Trans. Roy. Soc. A, Vol. 244 (822), (1952) 236-253.

Suhs, N. E. and Tramel, R. W., PEGSUS 4.0 Users Manual, Arnold Engineering Development Center Report, AEDC-TR-91-8, (1991), Arnold Air Force Station.

Author Profile

Hamn-Ching Chen: He received his Ph.D. degree in Mechanical Engineering in 1982 from The University of Iowa, Iowa City, Iowa, USA. He is an Associate Professor of Civil and Ocean Engineering of Texas A&M University. Before joining Texas A&M, he was a Research Scientist at Iowa Institute of Hydraulic Research from 1982 to 1988, and a Senior Research Scientist at the Marine Hydrodynamics Division of Science Applications International Corporation from 1988 to 1990. His research interests are in the development of numerical methods and turbulence models for prediction of submarine flows, ship berthing operations, bridge pier scour, body-wave-current interactions around coastal and offshore structures, and internal and film cooling of turbine blades.

Woei-Min Lin: He is currently the Division Manager of the Ship Technology Division of SAIC. Dr. Lin received his B.S. Degree in Naval Architecture and Marine Engineering (NA&ME) from the National Cheng-Kung University, Taiwan, in 1977. He received his M.S. and Ph.D. in Ocean Engineering from the Massachusetts Institute of Technology in 1982 and 1985 respectively. He also received a M.S. in Electrical Engineering and a M.S. in Technical Management from the Johns Hopkins University in 1990 and 1996 respectively. Dr. Lin has 22 years of experience in theoretical and computational fluid dynamics related to marine vehicles. Principal area of expertise is the development and application of physics-based predictive models and numerical simulation tools for dynamic and hydrodynamic performance of marine vehicles.